Application of Accelerated Polar Near-Field to Far-Field Transform to Plane-Bi-Polar Measurements

S.F. Gregson[1, 2], C.G. Parini[2]
[1] Next Phase Measurements LLC, CA, USA, stuart.gregson@qmul.ac.uk
[2] Queen Mary University London, London, UK

***Abstract*—the plane-bi-polar near-field measurement technique is a well-known and long-established method for determining far-field antenna patterns of medium to high gain antennas that is predicated on the use of a very simple positioning system that in essence comprises just two rotation stages. Hitherto, this technique has been comparatively sparsely deployed however the recent heightened interest in utilising articulated multi-axis industrial robots for the positioning systems of modern antenna test systems has similarly increased the amount of interest that this technique has received. This paper is an extension of the authors' prior work where here, for the first time, the recently developed efficient polar near-field to far-field transform is adapted to accommodate the plane-bi-polar case. The adapted plane-bi-polar non-interpolatory transform is developed with preliminary simulation results presented that verify the success of the efficient, novel, data processing technique. The requisite plane-polar sampling theorem is examined with implications on the computation of the corresponding Bessel series discussed.**

Index Plane-bi-polar, near-field, antenna measurements, Fourier, Bessel.

I. INTRODUCTION

The plane bi-polar near-field antenna measurement system [1, 2] is conceptually similar to the plane-polar [3, 4] case except here, the probe sweeps out a circular arc in two axes enabling the acquisition of samples across the surface of a conceptual flat disk, with that data typically being tabulated on a set of concentric rings. Mechanically, this is a comparatively simple positioning system to construct as the requirement for a linear translation stage is removed. The guided wave path is also drastically simplified as only two rotary joints are required to connect the RF output from the scanning near-field probe to the input of the network analyser to maintain the phase stability across the acquisition plane. Unfortunately, this mechanical simplification is achieved at the expense of increased computational effort and complexity. However, as we shall show, this may be overcome in a relatively straightforward manner. As the use of multi-axis industrial robots as probe positioners for near-field antenna measurements proliferates, so too has the interest in utilising these systems for the acquisition of plane-bi-polar near-field data. As multi-axis industrial robots position a tool, which in our case is an RF probe, through the rotation of a series of joints, *i.e.* rotation stages, this makes them sympathetic to plane-bi-polar measurements which inherently position the scanning near-field probe similarly through a set of rotations, and without the need to synthesise a virtual, linear, translation stage with a set of compound joint rotations.

An example test system comprising dual multi-axis industrial robots can be seen presented in Figure 1. Here, robot 1, R_1, is used for plane-polar radius (or diameter) scanning of the probe whilst robot 2, R_2, holds the antenna under test (AUT) with its boresight direction aligned vertical and is used to provide the 360° azimuthal axis rotation. However, if instead R_1 was to rotate joint J_1, *i.e.* the robot's base azimuth axis which is mounted on the vertical tower, and is furthest from the probe, then data would be acquired naturally in a plane-bi-polar mode with samples tabulated on a plaid, monotonic and equally spaced grid in β, α which denote the two rotation angles.

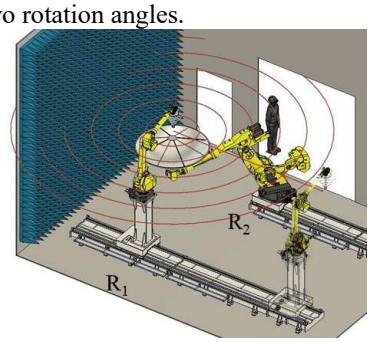

Fig. 1. Plane-polar antenna measurement using dual multi-axis robots used to acquire data tabulated on a plane-bi-polar coordinate system.

The success of this approach is clearly predicated upon the availability of a suitable near-field to far-field (FF) data transformation algorithm. A number of different algorithms have been proposed for the processing of plane-polar/bi-polar data and include the optimal sampling interpolation (OSI)/fast Fourier transform (FFT) [4, 5, 6] method, with non-interpolatory techniques including: Jacobi-Bessel transform [7], Fourier-Bessel transform [8], SVD-based transform [9] and pseudo-matrix inversion method [10] to name but a few. Recently, an accelerated plane-polar near-field to far-field transform has been proposed [11] which is in essence a generalization and refinement of the technique developed in [12] providing improvements in efficiency, flexibility and accuracy. In terms of the organization of this paper, Section II shows how the angular spectrum can be obtained from measurements taken in a plane bi-polar measurement system without recourse to approximation through an adaptation of [11]. Results are presented in

Section III and the paper concludes in Section IV with a summary, discussion and plans for future work.

II. Extension of Accelerated Plane-Polar Transform to Plane-Bi-Polar Measurements

The plane-polar and plane-bi-polar coordinate systems can be seen compared in Figure 2. Here, the data is assumed to be acquired uniformly at the intersection points between the radial (blue) and concentric (black) lines, with the corresponding unit vectors being denoted by the respective blue and black arrows where it is apparent that in each case, the data is acquired on a set of concentric rings. For the case of the plane-bi-polar system, the spacing between the adjacent rings changes as the "radial" scanning angle β is incremented from cut to cut. Furthermore, we can see that each ring is naturally "clocked", *i.e.* rotated, with respect to the preceding ring by some small angular amount, *cf.* also Figure 3. Specifically, as we shall show below, each ring is rotated by an angle $-\beta/2$. Thus, if we are to adapt the existing accelerated polar algorithm to accommodate the plane-bi-polar case both of these measurement artifacts will need to be accommodated within the data processing. Fortunately, and as will be shown below, this is a comparatively straight forward task.

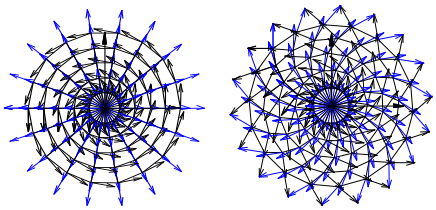

Fig. 2. Illustration of plane-polar (left) and plane-bi-polar (right) coordinate systems and unit vectors.

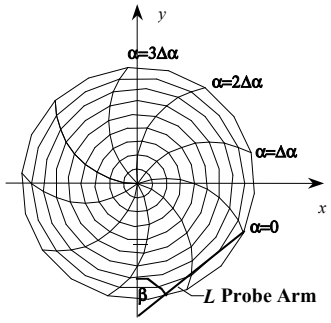

Fig. 3. Illustration of plane-bi-polar PNF measurement geometry.

Figure 3 presents a more detailed schematic of the plane-bi-polar measurement geometry which here also includes an illustration of how the, assumed fixed, probe arm length, L, is defined and relates to the two angular coordinates, β, α. The relationship between the plane-bi-polar coordinates as defined in Figure 3 and conventional Cartesian coordinates can be expressed as [1, 13],

$$x = L(\sin(\beta-\alpha)+\sin\alpha) \tag{1}$$

$$y = L(\cos(\beta-\alpha)-\cos\alpha) \tag{2}$$

Here z is arbitrary but assumed fixed during the acquisition, is typically a few wavelengths, and where the condition that $180° \geq \beta \geq 0$ applies. The relationship between the plane-bi-polar coordinates β, α and the (conceptually equivalent) plane-polar coordinates ρ, ϕ can be expressed compactly as [1],

$$\phi = \alpha - \beta/2 \tag{3}$$

$$\rho = 2L\sin(\beta/2) \tag{4}$$

Here, ρ and ϕ are the conventional radial and azimuthal plane-polar coordinates respectively. Intuitively, the relationship between the respective polar angles can be understood as when $\beta = 0°$ clearly $\phi = \alpha$. Similarly, when $\beta = 180°$, $\phi = \alpha - 90°$, and when $\beta = 90°$, $\phi = \alpha - 45°$, all of which can be seen from the geometry shown in Figure 3. From inspection of equation (3), we can see that each ring of plane-bi-polar data is clocked by an angle $-\beta/2$.

Considering the transform, by using the formula for a multidimensional exchange of variables we may express the plane-wave spectrum in terms of the plane-bi-polar near-field data as [13],

$$F(\theta,\phi) = L^2\int_0^{\pi}\int_0^{2\pi} f(\alpha,\beta)e^{jk_0(ux+vy)}\sin\beta\, d\alpha\, d\beta \tag{5}$$

Where, $u = \sin\theta\cos\phi$, $v = \sin\theta\sin\phi$ are direction cosines and x and y are given by equations (1) and (2) respectively. Similarly, and again by virtue of a multidimensional exchange of variables, we may express the plane-wave spectrum in terms of the plane-polar near-field data as [11, 13],

$$F(\theta,\phi) = \int_0^{2\pi}\int_0^{\infty} f(\rho',\phi')e^{jk_0\rho'\sin\theta\cos(\phi'-\phi)}\rho' d\rho' d\phi' \tag{6}$$

Here, primed variable denote near-field quantities. These expressions may be evaluated numerically as, by virtue of the sampling theorem, they can with no loss of accuracy be represented as a summation for the case where band-limited antennas are considered [11, 13, 14]. Crucially, for the plane-polar case, it was shown in [11] that the plane-wave spectrum can be obtained efficiently by evaluating,

$$F(\theta,\phi=\phi') = \Im^{-1}\left\{\sum_{n=1}^{N}\Im\left\{f(\rho_n',\phi')\rho_n'\right\} \cdot\Im\left\{e^{jk_0(\rho_n'\sin\theta\cos\phi')}\right\}\cdot\delta\rho'\delta\phi'\right\} \tag{7}$$

Here, $\Im$ denotes the Fourier transform operation, and $\Im^{-1}$ denotes the inverse operation with both of these being efficiently evaluated numerically using the mixed-radix FFT [14]. The corresponding far-electric-fields can be obtained from [11, 13],

$$\underline{E}(\theta,\phi) \approx \frac{j\cos\theta}{2\pi}\underline{F}(\theta,\phi)\frac{e^{-jk_0r}}{r} \tag{8}$$

An extensive validation of the accelerated plane-polar transform can be found presented in [11], together with an illustration of its successful application in the measurement of an electrically large x-band space-based planar SAR antenna, thus as a consequence of space constraints this will not be repeated herein and is instead left to the open literature. Probe compensated FF data can be obtained using standard planar probe pattern compensation [11, 13] providing a rotationally symmetrical, *i.e.* first order, probe

has been employed, or in the event that a probe with a more complex pattern is used, then the probe would need to be counter rotated during the near-field acquisition so as to remain polarization matched to the AUT when measuring each of the two orthogonal near-electric-field component [8], *cf.* a Ludwig 3 type acquisition [13]. Here, joint J_6 (*i.e.* the joint positioned closest to the probe) of the industrial robot, R_1, may be used to implement this counter-rotation with no further positioning hardware being necessitated. From inspection of equations (5) and (6), it is clear that their form is very similar suggesting that we will be able to adapt equation (7) to facilitate the processing of plane-bi-polar near-field data. The aforementioned rotation of each concentric ring by the angular amount $-\beta/2$ can be implemented conveniently, efficiently, and rigorously when the measured data is Fourier transformed, *cf.* Equation (7), and is a consequence of the shifting property of the Fourier transform [14]. Thus, the accelerated plane-bi-polar transform can be expressed as,

$$F(\theta,\phi=\alpha_{n=1}) = L^2\delta\beta\delta\alpha \cdot \Im^{-1}\left\{\sum_{n=1}^{N}\Im\left\{f(\beta_n,\alpha)\sin\beta_n\right\}e^{j\left(n-\frac{N}{2}-1\right)\frac{\beta_n}{2}}\Im\left\{e^{j2Lk_0\sin\theta\sin\left(\frac{\beta_n}{2}\right)}\right\}\right\} \quad (9)$$

Where there are N concentric rings of data within the near-field data set, and the elemental area of the points on the cut at $\beta = 0$ is a special case and is weighted as $\pi(\delta\beta)^2/(4N_\alpha)$. Each cut is assumed to have an angular span of $2\pi - 2\pi/N_\alpha$ and there are N_α equally spaced points in each concentric ring. Here we have assumed that the data provided by the one dimensional Fourier transform places the DC frequency component at the centre of the spectrum. The complex exponential factor that is within the summation is used to account for the clocking of the plane-bi-polar near-field data, the $\sin\beta_n$ term, *cf.* equation (5), is used to compensate for the variation in widths of the concentric rings, and the complex exponential within the final Fourier transform is modified for the position of the plane-bi-polar data points, *cf.* equations (1), (2) and (4).

As was previously the case, the efficiency derives from the use of the mixed-radix one-dimensional fast Fourier transform (FFT) algorithm, with the rigor and robustness stemming from the avoidance of recourse to approximation. Note, zero-padding a factor of 2 FFT can yield erroneous results. This is also the reason for the requirement that the data is periodic in the α-axis, *cf.* spherical case, and does not span the full 2π radian range with redundant points at both $\alpha = 0$ and $\alpha = 2\pi$. Lastly, this transform is numerically equivalent to a discrete Fourier transform, but is *circa* three orders of magnitude faster, and can transform measurements of electrically large antennas to the FF in a few seconds on a modern workstation. In summary then, the new accelerate plane-bi-polar transform is based on the following assumptions: 1) a rotationally symmetric first order probe is used, or the probe is counter rotated during the near-field acquisition [11], 2) the data is acquired using fixed $\delta\beta$ and $\delta\alpha$ per α cut. Note, this assumption is common to many transforms and is not a limitation of this particular implementation per se, and 3) a positive (suppressed) time dependency is assumed. The next section presents results obtained from this new transform.

III. Results

The use of this accelerated polar transform can be illustrated by taking simulated plane-bi-polar near-field data and transforming it to the FF whereupon it can be compared with FF obtained directly from the antenna simulation software. Figure 4 presents simulated measured plane-bi-polar near-electric-field components of a parabolic reflector antenna with an elliptical cross-section measuring 0.4 m by 0.3 m, and radiating at 5.0 GHz for the two orthogonal tangential polarizations E_x (left) and E_y (right), and where an arm length $L = 2.0$ m was used. Here, the horizontal axis is the measurement "radius" variable β, and the vertical axis corresponds to the azimuthal angle α, where both are expressed in degrees. The AUT to probe separation was 0.6 m (*circa* ten wavelengths) yielding an estimated maximum pattern angle of approximately ±70°. The algorithm developed above was then employed to transform the plane-bi-polar near-electric-field data to the FF with the resulting far-fields being compared to data provided directly from reflector antenna simulation software. Here, an off-pointed reflector antenna was employed where the rotation of the antenna with respect to the acquisition axes was deliberately included to make sure that any natural symmetry within the simulated measurement would be broken to further aid the verification process [11].

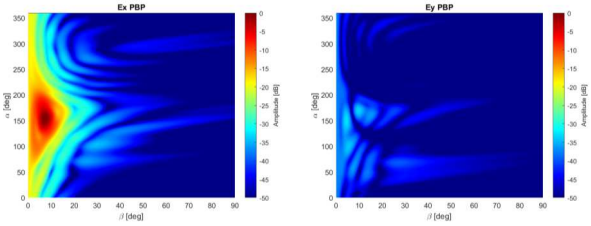

Fig. 4. Illustration of plane-bi-polar *x*-polarised near electric field component (left) and *y*-polarised field component (right).

Here, the sequential clocking of the plane-bi-polar near-field data is evident from the "sloping" trails of sidelobes that are visible in Figure 4, and is a measurement artefact that is absent from equivalent plane-polar measurements, and the corresponding transformed FF patterns.

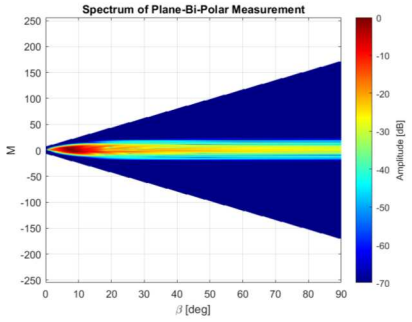

Fig. 5. False colour plot of power in Fourier coefficients plotted as a function of "radius" variable β.

This is the phenomena that the complex exponential factor embodied in equation (9) seeks to address. Figure 5 presents a false-colour checkerboard plot of the intensity of the corresponding Fourier coefficients of the plane-bi-polar data. We shall now examine this in the context of the sampling theorem. The standard plane-polar, sampling criteria in the angular (*i.e.* azimuthal) axis can be expressed as [6, 11, 15],

$$\Delta\alpha = \frac{\lambda}{2(a+\lambda)} = \frac{\pi}{M} \tag{10}$$

Here, the parameter a denotes the maximum radial extent (MRE). This is the radius of a circle that encloses the AUT, *i.e.* the majority of the current sources, which is measured from the centre of α rotation. The addition of a wavelength, *i.e.* one λ, is included to make sure that sufficient Fourier terms are included in the representation. However, this value may be increased if greater accuracy is required. Clearly, the MRE has to be less than the maximum radius of the acquisition disk if truncation is to be negligible. However, if the AUT is known to be rotational symmetric, then larger data point spacing may be adopted without introducing unacceptable errors. Here, M can be interpreted as representing the maximum order of Bessel function which we can use to place an upper limit on the maximum number of Fourier terms required [11], *cf.* equation (11) below. This can also be seen from Figure 5, where the largest power is contained within only the lower order Fourier coefficients, *i.e.* we see a horizontal-band that is centred about $M = 0$. In this case, the MRE of the antenna was 0.2 m corresponding to a maximum mode of $M_{Max} = 28$ [13]. From inspection of this figure we see that the majority of the power is contained within those coefficients for which $|M| < 28$.

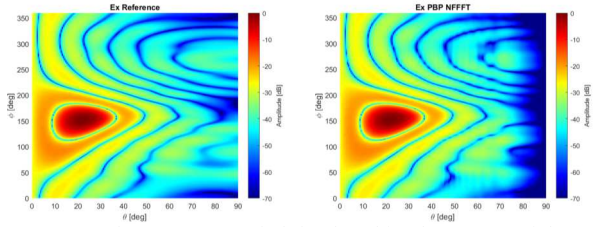

Fig. 6. FF x-pol amp pattern, ref. (left) plane-bi-polar NFFFT (right).

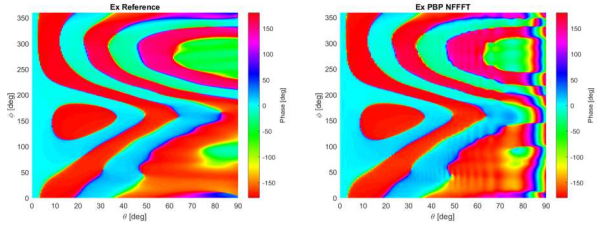

Fig. 7. FF x-pol phase pattern, ref. (left) plane-bi-polar NFFFT (right).

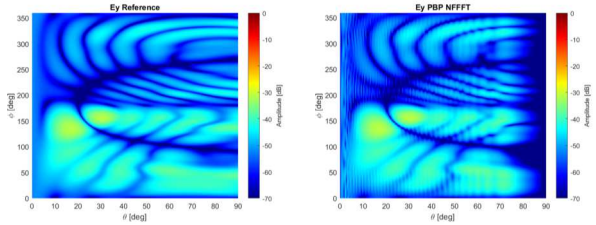

Fig. 8. FF y-pol amplitude pattern, ref. (left) plane-bi-polar NFFFT (right).

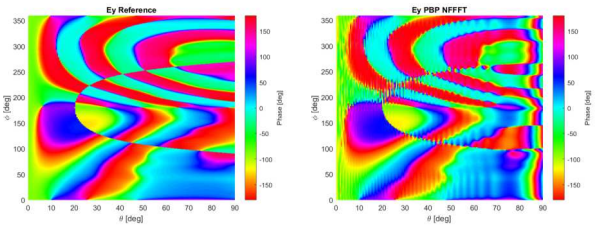

Fig. 9. FF y-pol phase pattern, ref. (left) plane-bi-polar NFFFT (right).

The plane-bi-polar near-field data was transformed to the FF using equation (9). Figure 6 (left) presents the FF of the x-polarized far-fields plotted as a false-colour checkerboard plot tabulated on a regular polar-spherical coordinate system of the parabolic reflector antenna. The right hand side of Figure 6 contains an equivalent plot of the FF obtained from the new plane-bi-polar transform. Here, similarly, Figure 7 presents the equivalent x-polarised phase plots with Figures 8 and 9 containing the equivalent y-polarised amplitude and phase patterns respectively. From inspection of these plots is it clear that the results are in encouraging agreement. The differences which can be seen here are a result of the first and second order truncation effects [13]. Thus, the attenuation of the pattern at wide out angles is a consequence of the finitely large acquisition disk (1st order truncation effect onset at ~70°) and the ripple that is evident across the pattern is due to spectral leakage (2nd order truncation effect). This second effect is most evident on the cross-polar pattern shown at the right-hand side of Figure 8. By way of a further comparison, Figure 10 contains iso-level, *i.e.* contour, plots of the x- and y-polarised FF amplitudes. Here, red contours denote the reference FF pattern (truncation free) and the black contours are the equivalent patterns obtained from the plane-bi-polar transform. Again, the agreement is very encouraging.

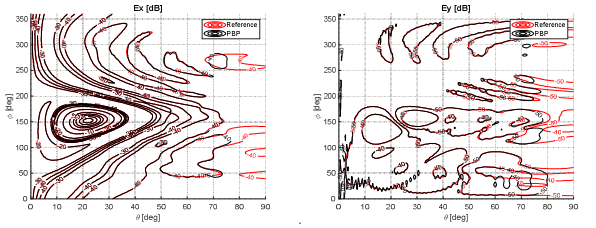

Fig. 10. FF comparison iso-level plot of x-polarised amplitude (left), y-polarised amplitude (right).

As suggested by equation (10), for the case of an electrically large antenna, a large number of high-order Bessel functions are required to be computed since, and as is also the case for the plane-polar transform, the Fourier transform of the complex exponential is computed analytically from a truncated infinite series [11],

$$\Im\left\{e^{j\chi\cos\alpha}\right\} = n_\alpha\left[J_0(\chi), jJ_1(\chi), j^2J_2(\chi), j^3J_3(\alpha), \ldots, j^3J_3(\alpha), j^2J_2(\chi), jJ_1(\chi)\right] \tag{11}$$

This enables the rapid, accurate, implementation of this transform. Bessel functions, such as these, are generally computed using recurrence relations requiring only the first couple of terms in the series to be directly computed, with all other terms being obtained from these values [16]. Although this means that we can determine *all* of the values needed

very efficiently, it does present some difficulties computationally. For the case where the argument, χ, is larger than the order of the Bessel function, we may use an "upwards" recurrence from J_0 and J_1 which is always stable. Unfortunately however, when the argument, χ, is smaller than the order we utilize a "downwards" recurrence relation which can suffer from numerical overflows and the resulting instabilities. Thus, we are required to renormalize the values for the recurrence relations to remain within the available machine precision. Thus, when the recurrence is completed, we are able to correct the result for the various renormalization(s) that were applied during the iteration and thereby obtain reliable values. This it turns out, is not only a more efficient strategy than the brute force approach of computing a large number of (likely) mixed-radix 1D FFTs, it is also superior in terms of accuracy and precision.

IV. Summary and Conclusions

As we have shown, the recently developed accelerated polar near-field to far-field transform [11] can be readily adapted so that it is amenable to processing plane-bi-polar measured data with no loss in computational efficiency or rigour. This transform is rigorous, *i.e.* it does not rely upon approximation, the solution of a linear system of simultaneous equations, least squares fitting, *etc*. Although the FF data will be provided tabulated on an equally spaced grid of points in the azimuthal-axis (that will contain a power of 2 points if zero-padded to increase resolution [11]) the user is free to specify the number and location of points in the θ-axis. Preliminary simulated data was used to validate and verify the novel transform against a known truth model with very encouraging results attained. Although an off-pointed reflector antenna was used as the basis of these measurement simulations, this technique is equally applicable to other types of antenna and different frequency bands providing only that the majority of the radiated field is sampled by the near-field measurement, *i.e.* the antennas have some gain, *e.g.* ideally *circa* 15 dB or greater, and that the measurements are acquired outside of the reactive region, which is in common to other planar near-field methods. Since the transformation is based upon the standard plane-wave spectrum technique, the method is no more sensitive to the impact of measurement errors. Arguably, if the same number of points are acquired in each concentric ring, then the oversampling this provides helps improve measurement quality as the averaging can aid in the resilience of the technique to some forms of error, *e.g.* random sources and some forms of scattering. Clearly, the lack of reliance upon approximation within the transform technique also aids in its robustness. However, this is an area of future work which is include examining in greater detail the behavior of the Fourier coefficients in the presence of noise with the intention of exploring possible ways that this can be used to further improve the accuracy of the measurement by extracting multiple-reflections *etc*. as well as to obtain additional experimental validation.

References

[1] L.I. Williams, Y. Rahmat-Samii, R.G. Yaccarino, "The Bi-Polar Planar Near-Field Measurement Technique, Part I: Implementation and Measurement Comparisons", IEEE Trans. Antennas Propagat., vol. AP-42, February 1994.

[2] R.G. Yaccarino, Y. Rahmat-Samii, L.I. Williams, "The Bi-Polar Planar Near-Field Measurement Technique, Part 11: Near-Field to Far-Field Transformation and Holographic Imaging Methods", IEEE Trans. Antennas Propagat., vol. AP-42, February 1994.

[3] Y. Rahmat-Samii, V. Galindo-Israel and R. Mittra, "A plane-polar approach for far-field construction from near-field measurements," IEEE Trans. Antennas Propagat., vol. AP-28,pp. 216-230, March 1980.

[4] O.M. Bucci, C. Gennarelli, C. Savarese, "Fast and accurate near-field-far-field transformation by sampling interpolation of plane polar measurements," IEEE Trans. Antennas Propagat., vol. AP-39, pp. 48-55, January 1991.

[5] F. D'Agostino, F. Ferrara, C. Gennarelli, R. Guerriero, M. Migliozzi, "Laboratory Tests on a NF-FF Transformation Technique from Nonredundant Bi-Polar Data", 2016 Loughborough Antennas & Propagation Conference (LAPC), UK.

[6] F. D'Agostino, R. Guerriero, F. Ferrara, M. Migliozzi, "Evaluation of the Far Field Radiated by a Flat AUT from Non-Redundant Near-Field Bi-Polar Samples", 2022 Microwave Mediterranean Symposium (MMS), 2022.

[7] V. Galindo-Israel and R. Mittra, "A new series representation for the radiation integral with application to reflector antennas," IEEE Trans. Antennas Propagat., vol. AP-25, pp. 631-641, September 1977.

[8] R. Mittra, W.E. Ko, M.S. Sheshadri, "A transform technique for computing the radiation pattern of prime-focal Cassegrainian reflector antennas," IEEE Trans. Antennas Propagat., vol. AP-30, pp. 520-524, May 1982.

[9] F. D'Agostino, F. Ferrara, C. Gennarelli, R. Guerriero, M. Migliozzi, "Laboratory Testing of a SVD-Based Approach to Recover the Nonredundant Bi-Polar NF Data from the Positioning Error Affected Ones", Loughborough Antennas & Propagation Conference (LAPC 2017), UK.

[10] C.G. Parini, S.F. Gregson, J. McCormick, D. Janse van Rensburg, T. Eibert, "Theory And Practice of Modern Antenna Range Measurements 2nd Expanded Edition, Volume 1", IET Electromagnetic Waves series 55 ISBN 978-1-83953-126-2, January 2021 UK.

[11] S.F. Gregson, C.G. Parini, B. Pyne, H. Saito, K. Tanaka, "Highly Efficient Near-Field to Far-Field Transform for Polar Near-Field Scanned Data", Antenna Measurement Techniques Association, Annual symposium and meeting, October, 2022, Denver, Colorado, USA.

[12] J.C. Bennett, "Fast Algorithm for the Calculation of Radiation Integral and its Application to Plane-Polar Near-Field/Far-Field Transformations", Electronic Letters, 11th April 1985, Vol. 21 No. 8, pp. 343-344.

[13] S.F. Gregson, J. McCormick, C.G. Parini, "Principles of Planar Near-Field Antenna Measurements", IET Press, 2007, pp. 93, ISBN 978-0-86341-736-8.

[14] A.V. Oppenheim, R.W. Schafer, "Discrete-Time Signal Processing", New Jersey, Prentice Hall, 1989.

[15] A.D. Yaghjian, "An Overview of Near-Field Antenna Measurements", IEEE Trans., 1986, AP-34, pp. 3 W 5.

[16] W.H. Press, B.P. Flannery, S.A. Teukolsky, W.T. Vetterling, "Numerical Recipes in FORTRAN 77, The Art of Scientific Computing 2nd Edition", Cambridge University Press, 1993, ISBN 9780521430647.